

DCIts - Deep Convolutional Interpreter for time series

Domjan Barić, Davor Horvatić*

*^aDepartment of Physics, Faculty of Science, University of Zagreb, Bijenička cesta
32, Zagreb, 10000, Croatia*

Abstract

We introduce an interpretable deep learning model for multivariate time series forecasting that prioritizes both predictive performance and interpretability—key requirements for understanding complex physical phenomena. Our model not only matches but often surpasses existing interpretability methods, achieving this without compromising accuracy. Through extensive experiments, we demonstrate its ability to identify the most relevant time series and lags that contribute to forecasting future values, providing intuitive and transparent explanations for its predictions. To minimize the need for manual supervision, the model is designed so one can robustly determine the optimal window size that captures all necessary interactions within the smallest possible time frame. Additionally, it effectively identifies the optimal model order, balancing complexity when incorporating higher-order terms. These advancements hold significant implications for modeling and understanding dynamic systems, making the model a valuable tool for applied and computational physicists.

Keywords:

Multivariate Time Series Forecasting, Interpretable Deep Learning, Model Interpretability, Mechanistic Interpretability

1. Introduction

Forecasting multivariate time series and uncovering the underlying dynamics presents a significant challenge not only in physics but across various domains, including finance, healthcare, and environmental monitoring. In

*davorh@phy.hr

these areas, accurate forecasting is critical for decision-making, as minor errors can lead to significant consequences. Recently, deep learning models have demonstrated superior performance in multivariate time series forecasting, outperforming traditional statistical models in prediction accuracy [1]. However, the inherent complexity and opaque nature of these models obscure the understanding of their predictive processes. This obscurity in model interpretability severely restricts their applicability in scenarios where understanding the rationale behind predictions is paramount, such as in healthcare, where ensuring patient safety depends on comprehending the predictive reasoning.

In response to this interpretability challenge, there is an increasing interest in developing deep learning models for time series forecasting that offer greater interpretability. Such models strive to shed light on their decision-making processes by pinpointing and emphasizing the significance of the most relevant features within the input series, thereby elucidating their influence on the final predictions.

The research conducted by Barić et al. [2] delves into the domain of interpretable models for multivariate time series analysis, providing a review of the current landscape. To aid in the analysis and comparison of these models, the authors have developed benchmarking datasets intended as a standard for evaluation. Moreover, they utilised a Performance-Explainability Framework that assesses models based on various criteria such as performance, comprehensibility, granularity, information, faithfulness, and end-user considerations, enabling a detailed evaluation of these models [3]. The findings from this study suggest that while the evaluated models generally exhibited satisfactory performance in terms of prediction accuracy, their interpretability often lagged, rendering them less trustworthy. Notably, only one model, the IMV-LSTM [4], showed promise in interpretability but failed to deliver consistent performance across multiple datasets. The IMV-LSTM model innovates by utilizing the hidden state matrix and devising an update scheme where each element (e.g., row) of the matrix exclusively captures information from a specific input feature, aiming to enhance interpretability.

In recent years, there have been multiple efforts to create interpretable or explainable neural networks for time series forecasting tasks. Beyond the attention mechanism discussed by [2], researchers have explored model-agnostic approaches [5, 6] such as SHAP [7] and perturbation methods [8]. Attention mechanisms, in particular, have demonstrated the potential to yield interpretable predictions by highlighting the most relevant features in

the input series. These mechanisms have been incorporated into various deep learning models, including recurrent neural networks (RNNs), convolutional neural networks (CNNs), and transformers, to facilitate interpretability in multivariate time series predictions.

The use of attention weights to evaluate attention models is widespread, offering insights into which segments of the data are deemed crucial by the model. There exist numerous instances where the attention mechanism is utilized for enhancing interpretability, specifically within the realm of time series analysis [9, 10, 11, 12, 13, 14]. Despite this, the application of attention weights to identify significant data parts has sparked debates regarding the meaningfulness of the explanations provided by attention. The paper "Attention is not Explanation" [15] argues that attention weights do not necessarily align with the crucial features, highlighting that models can arrive at identical conclusions despite varying attention distributions. Contrarily, the paper "Attention is not not Explanation" [16] contests this view, demonstrating that attention weights, when informed through learning, outperform those generated by adversarial distributions. Thus, researchers must approach the interpretation of attention patterns with caution, as these weights might offer plausible insights into the model's focus areas without definitively indicating the significance of data parts. Furthermore, the efficacy of this method is influenced by the specific architecture of the model.

The other approach is to adapt model architectures to be inherently interpretable by design. Oreshkin et al. [17] introduced N-BEATS, a neural network tailored for univariate time series forecasting, which incorporates interpretability through explicit trend and seasonality decomposition, achieving this with minimal accuracy loss. However, its application is limited to univariate data and predefined trend and seasonality components, lacking in causal analysis between data points. Ozyegen et al. [5] proposed DANLIP, a model designed for joint density parameter estimation by conducting time step-wise parameter forecasts. This model, focusing on Gaussian stochastic processes, utilizes a preprocessing module with encoder and decoder modules to estimate the mean and standard deviation of the Gaussian distribution. While enhancing interpretability, these models impose significant restrictions and do not address causality. Rasul et al. [18] developed a model utilizing conditioned normalizing flows to model the covariance matrix, thus highlighting feature importance within its architecture. Despite these advancements, such models still overlook the temporal dynamics inherent in time series data. Munkhdalai et al. [19] and Panja et al. [20] employed a hybrid ap-

proach that combines simpler models with deep learning components, yet these methods lacked mechanisms for interpreting the deeper aspects of the models. Fauvel et al. [21] introduced XCM, an eXplainable Convolutional neural network that extracts information relevant to the observed variables and time, enabling the application of model-specific post hoc explainability methods to achieve both temporal and spatial interpretability. Similarly, Assaf et al. [22] and Wang et al. [23] developed the Multilevel Wavelet Decomposition Network, a frequency-aware deep learning model that performs hierarchical decomposition of time series into wavelets, geared towards time series classification. Despite the novelty of these approaches, they still lack in providing causal relationships between different time steps and series.

The paper "Time series causal relationships discovery through feature importance and ensemble models" [24] introduces innovative methods that leverage the power of ensemble models and feature importance analysis to discern causal relationships within multivariate time series data. Ensemble models, known for their robustness and accuracy, combine predictions from multiple machine learning algorithms to improve predictive performance. In this context, they are used to analyze complex time series data more effectively than single-model approaches. Although an interesting approach provides causality for each time series and each lag, it does not provide insight into how the source time series impacts the target time series, it only shows that causality exists. Also, it uses feature importance from ensemble models which is not easily explained. Finally, this approach requires time series to be detrended, which can potentially obscure some causalities in data. This also makes the result depend on the detrending technique and hyperparameters.

In the following section, we present a deep-learning model designed specifically for forecasting multivariate time series. The design of this model emphasizes both forecast accuracy and interpretability. Our findings reveal that this model not only meets but also exceeds the interpretability of current models without sacrificing forecast precision. To minimize the need for manual supervision, the model is designed so one can robustly determine the optimal window size that captures all necessary interactions within the smallest possible time frame. Additionally, it effectively identifies the optimal model order, balancing complexity when incorporating higher-order terms.

Through detailed experiments, we demonstrate the model's ability to identify the most significant time series, their order and lags, offering clear and simple rationales for its forecasts.

2. Deep Convolutional Interpreter of time series

We introduce a novel architecture designed for modeling multivariate time series (MTS). An MTS system consists of N time series, each of length M , collectively represented by $\mathbf{X} = \mathbf{X}_1, \mathbf{X}_2, \dots, \mathbf{X}_N$. The n -th time series in this system is denoted by $\mathbf{X}_n = (X_{n,1}, X_{n,2}, \dots, X_{n,M})$, where $X_{n,t} \in \mathbb{R}$ signifies the value of the n -th time series at time t . Here, $n = 1, 2, \dots, N \in \mathbb{N}$ indexes the series, and $t = 1, 2, \dots, M \in \mathbb{N}$ indexes time points within each series. We aim to analyze and decipher the interactions among various time series and their respective lags. We have developed a deep convolutional interpreter for time series (DCItS) to achieve this. This architecture is designed to approximate the transition operator α , which describes how the time series evolves between consecutive time points, utilizing the L lags in the MTS window \mathbf{Q}_t :

$$\mathbf{X}_{t+1} = \alpha \mathbf{Q}_t, \quad (1)$$

therefore the initial step in applying DCItS to multivariate time series (MTS) involves a windowing technique. We define a fixed-size window, L , with $L < M$, to segment MTS into overlapping intervals. We construct a sequence of windows, denoted as \mathbf{Q}_t . Each window \mathbf{Q}_t is defined as:

$$\mathbf{Q}_t = (\mathbf{X}_{t-L+1}, \dots, \mathbf{X}_{t-2}, \mathbf{X}_{t-1}, \mathbf{X}_t), \quad \text{for } t = L, L+1, \dots, M. \quad (2)$$

In machine learning terms, we represent our dataset as $\mathbf{Q} \in \mathbb{R}^{(M-L+1) \times N \times L}$, where the first dimension denotes the number of samples within our dataset, and \mathbf{Q}_t signifies an individual sample¹. The objective of DCItS is to approximate the transition operator α for each sample \mathbf{Q}_t . For this purpose, DCItS utilizes a tensor α , with $\alpha \in \mathbb{R}^{N \times N \times L}$. The tensor α dimensions are aligned with those of a single sample \mathbf{Q}_t , where the first two dimensions represent the interaction between time series, and the third dimension corresponds to the lag or time step. Hence, $\alpha_{n,i,j}$ explains the impact of the i^{th} time series at lag j on the subsequent value of the n^{th} time series at time $t+1$.

The transition equation (1) encapsulates this relationship:

$$X_{n,t+1} = \sum_{i=1}^N \sum_{j=1}^L (\alpha \diamond \mathbf{Q}_t)_{n,i,j}. \quad (3)$$

¹It is important to ensure that samples \mathbf{Q}_t that contain overlapping data due to the rolling window are not included in the training, validation, and test sets during the train/validation/test split.

The operator \diamond denotes element-wise multiplication (Hadamard product) augmented with broadcasting:

$$(\boldsymbol{\alpha} \diamond \mathbf{Q}_t)_{n,i,j} = \alpha_{n,i,j} \times Q_{n,j}, \quad (4)$$

where $\boldsymbol{\alpha} \diamond \mathbf{Q}_t \in \mathbb{R}^{N \times N \times L}$ represents the resultant tensor over which we sum. Through broadcasting, \mathbf{Q}_t is replicated across the tensor $\boldsymbol{\alpha}$'s first dimension, facilitating the requisite element-wise multiplication.

Moreover, this tensor allows an interpretation of the MTS system's internal dynamics. Specifically, it enables deciphering of the underlying equations that generate the MTS.

To realize its objectives, DCIts employs a two-step predictive strategy. The initial phase dubbed the *Focuser*, is tasked with identifying significant lags and time series - effectively separating the signal from noise. Following this, the *Modeler* phase leverages the insights from the Focuser, alongside the original input, to deduce the final coefficients for the transition tensor $\boldsymbol{\alpha}$. The final result is calculated using input, Focuser, and Modeler output. The architecture of the network is shown in Figure 1. Many models with

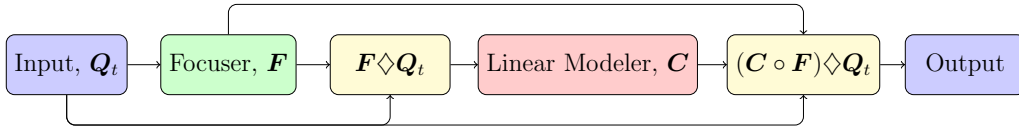


Figure 1: Figure shows a high-level architecture of DCIts, which consists of two modules, Focuser and linear Modeler. Focuser uses input to calculate the most important data points, i.e. tries to find which parts impact output. The linear Modeler calculates linear coefficients for each time series and lag, which are used to calculate the next step in the time series. The final result \mathbf{X}_t is calculated as the product of input, Focuser output and Modeler output. In Section 2.4 we show how to extend the architecture to include nonlinear parts.

inherent interpretability have two steps in their architecture [25, 26], but they focus on decoupling autocorrelation from cross-correlation, which limits the model's capacity to understand subtleties that can be present in the data. With DCIts, we also use two steps to achieve interpretability, but we do not decouple the estimation of autocorrelation from cross-correlation.

2.1. Focuser and Modeler

Both the Focuser and Modeler use the same overall architecture (shown in Figure 2), the only difference is in the final layer.

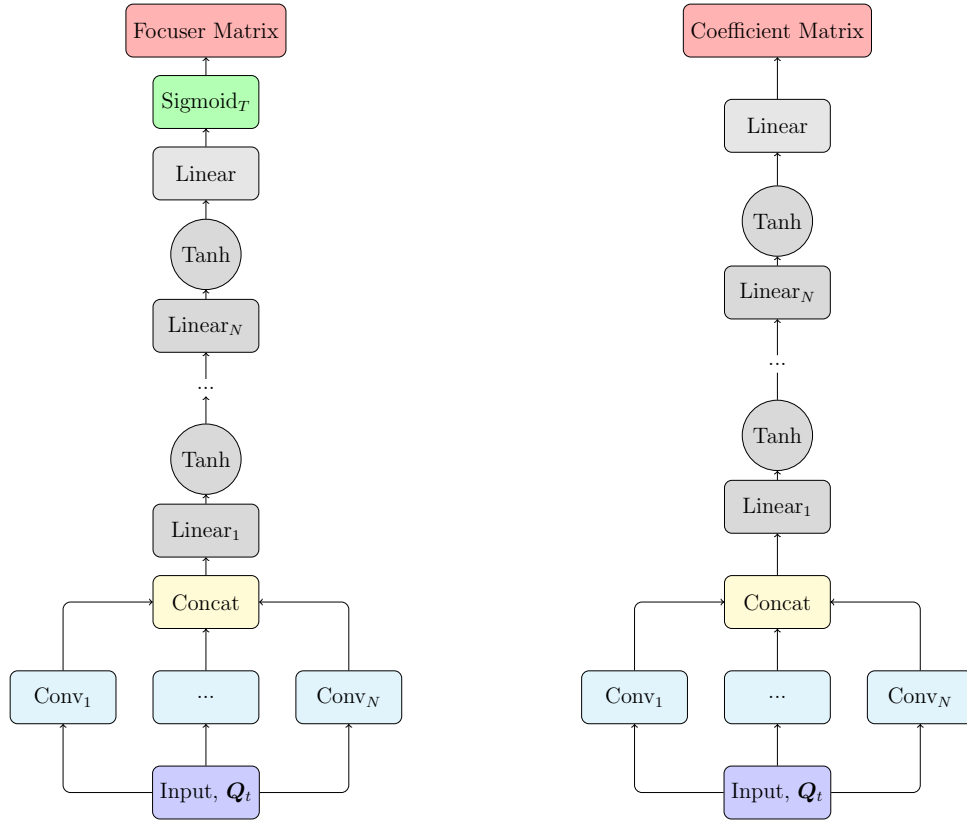


Figure 2: The left figure illustrates the architecture of the Focuser, while the right figure depicts that of the Modeler. Observing their structures, we find a notable similarity in their foundational design. Each begins with a sequence of convolutional layers, which are subsequently concatenated and directed into a succession of fully connected linear layers activated by tanh functions. However, a difference is present in the final layer: the Focuser employs a sigmoid function to eliminate inputs of lesser importance, effectively distinguishing between noise and signal. Conversely, the Modeler is devoid of any activation function, aimed at calculating coefficients for every input value. This aspect of the Modeler aligns it closely with the principles of linear regression, treating inputs as variables within such a framework. The absence of an activation function is deliberate, ensuring that the modeling of coefficients remains unrestricted. This is crucial, for instance, in modeling anti-correlation, which would not be feasible with the application of *ReLU* or similar activation functions.

In both Focuser and Modeler, we first apply a set of convolutional kernels with varying shapes. There is no need for advanced and more complex neural network layers. Currently, state-of-the-art models use attention layers, however, we believe that we would lose some of the capabilities if we were to use attention.

Convolutional layers employed in the presented model, each characterized by distinct dimensions that cater to different aspects of the time series data are:

- Global Convolutional Layer: Dimension $N \times L$ - Processes across all time series with window length L .
- Time Convolutional Layer: Dimension $1 \times L$ - Focuses on temporal patterns within a single window across all series.
- Time Series Convolutional Layer: Dimension $N \times 1$ - Captures features across all time series at a single time point.
- First Neighbour Layer: Dimension $N \times 3$ - Analyses each time series and its immediate neighbours.
- Second Neighbour Layer: Dimension $N \times 5$ - Extends the analysis to include second-order neighbours for each series.
- Single Time Series First Neighbour Layer: Dimension 1×3 - Isolates a single series to examine it with its immediate neighbours.
- Single Time Series Second Neighbour Layer: Dimension 1×5 - Further isolates a single series for analysis with its second-order neighbours.

This structured approach allows for a comprehensive analysis of both global and local dynamics within the multivariate time series data. After applying the convolutional layers, we concatenate the results.

$$\mathbf{K}_m = \text{Conv}_m(\mathbf{Q}_t), \quad m = 1, 2, \dots, C_N, \quad (5)$$

$$\mathbf{K} = \text{Concat}([\mathbf{K}_1, \mathbf{K}_2, \dots, \mathbf{K}_{C_N}]). \quad (6)$$

The resulting tensor is then passed through three fully connected layers activated by tanh functions, yielding the output $\mathbf{H} \in \mathbb{R}^{N \times N \times L}$. This means that each time series in the system generates a matrix mirroring the input's shape. The rationale for this specific output structure is to create a transition tensor for each time series, with the output's first dimension enabling

iteration over the input time series. This can be summarized with:

$$\mathbf{H} = \tanh(\mathbf{W}_{H_N} \tanh(\dots \mathbf{W}_2 \tanh(\mathbf{W}_1 \mathbf{K} + \mathbf{b}_1) + \mathbf{b}_2) + \mathbf{b}_{H_N}). \quad (7)$$

The number of convolutional layers C_N , and the number of fully connected layers H_N can vary and can be adjusted for specific MTS systems. The final layer is the linear layer which is used to calculate Modeler tensor $\mathbf{C} \in \mathbb{R}^{N \times N \times L}$:

$$\mathbf{C} = \mathbf{W}_H \mathbf{H} + \mathbf{b}_H. \quad (8)$$

With tensor \mathbf{C} we want to obtain the amplitude and the sign of the α elements. Tensor \mathbf{C} can have negative values modelling any anti-correlations that exists in the system. Furthermore, higher values (in absolute meaning) suggest a higher impact on the output.

We applied a standard methodology for subset selection to all combinations of the listed convolutional layers, initially using Mean Squared Error (MSE) as the loss function for the forecasting task, followed by Mean Absolute Error (MAE). We varied the hidden layer count for each instance, H_N , from 1 to 5. To ensure robustness, we repeated this process five times for each combination. We confirmed the robustness of our model’s forecasting power and interpretability, concerning the subset selection of convolutional layers and the number of fully connected layers on test data, as will be discussed in the next section. Importantly, the choice of the loss function can influence slightly the confidence in interpretability in specific cases that are easy to detect. Therefore, for the remainder of this paper, we will employ all seven convolutional layers and three fully connected layers ($H_N = 3$).

It’s important to note that this type of analysis can be repeated to tailor the selection and construction of convolutional layers and the number of hidden layers to suit the specific data. We suggest starting with the same setup of seven convolutional layers and three fully connected layers, as we have consistently achieved reliable results with this configuration in all our experiments.

For Focuser we apply a pointwise sigmoid function which produces tensor \mathbf{F} :

$$\mathbf{F} = \sigma_T(\mathbf{H}). \quad (9)$$

Where $\sigma_T(x)$ represents the temperature depended sigmoid function:

$$\sigma_T(x) = \frac{1}{1 - e^{-x/T}}.$$

The elements of tensor \mathbf{F} range between 0 and 1, denoted as $F_{i,j,k} \in (0, 1)$. The purpose of tensor \mathbf{F} is to differentiate between noise and signal, aiding the model in identifying which segments of \mathbf{Q}_t warrant attention. In this paper we will set $T = 1$, we did extensive analysis on the influence of temperature and we see potential benefits if one wants to further suppress non-significant elements but in present benchmarking datasets, we did not see any benefit in changing the default temperature.

The difference between Modeler and Focuser is in the input. The Modelers input is not \mathbf{Q}_t , but $\mathbf{F} \diamond \mathbf{Q}_t$. Finally, to get model output, we need to multiply input with both tensor \mathbf{F} and tensor \mathbf{C} :

$$X_{n,t+1} = \sum_{i,j}^{N,L} ((\mathbf{C} \circ \mathbf{F}) \diamond \mathbf{Q}_t)_{n,i,j} \quad (10)$$

where \circ is Hadamard product generalized to higher order tensors:

$$(\mathbf{C} \circ \mathbf{F})_{i,j,k,\dots} = C_{i,j,k,\dots} \times F_{i,j,k,\dots} \quad (11)$$

By comparing equation (3) and (10) we can see that:

$$\boldsymbol{\alpha} = \mathbf{C} \circ \mathbf{F} \quad (12)$$

The transition tensor is the Hadamard product of Focuser output \mathbf{F} and Modeler output \mathbf{C} , with interpretability already incorporated into DCIts. The model can not make predictions without giving learned interpretability. We achieved the whitening of the complex black-box model. Furthermore, tensors \mathbf{F} and \mathbf{C} are produced for each example both during the training and prediction (testing) phase. We can locally understand why the model made each prediction. Interpretability given by the model is not averaged over all examples as averaging could lose some aspects of the dynamics. The model produces an interpretability for every single sample.

2.2. Interpretability

We refer to the transition tensor $\boldsymbol{\alpha}$ to maintain consistency with the notation used in related literature, we will also refer to the transition tensor as $\boldsymbol{\alpha}$ coefficients when discussing model interpretability. Given that we have a set of $N - L + 1$ samples, there will be an equal number of $\boldsymbol{\alpha}$ coefficients, each corresponding to a specific sample, denoted as $\boldsymbol{\alpha}_t$. Throughout the remainder of this paper, unless otherwise specified, any reference to $\boldsymbol{\alpha}$ coefficients or

derived quantities pertains to the coefficients from the individual sample α_t , $\alpha_t \in \mathbb{R}^{N \times N \times L}$.

The model’s α coefficients quantify the influence of all time series, including self-influence, on the final output at each time point t within the window, i.e. modeling the next step in the time series, as we discussed previously. Algorithm 1 provides full details on extracting interpretability. To enhance the performance of interpretability, it is generally advisable to shuffle the training set.

To focus solely on the mutual influence among time series, while setting aside the temporal aspect of their interactions, we introduce the $\tilde{\beta}$ and β coefficients. Both $\tilde{\beta}$ and β have dimensions $\mathbb{R}^{N \times N}$, allowing us to analyze the relative impact between time series without directly considering the time lag of these interactions:

$$\tilde{\beta}_{i,j} = \sum_{l=1}^L |\alpha_{i,j,l}|, \quad (13)$$

$$\beta_{i,j} = \frac{\tilde{\beta}_{i,j}}{\sum_{k=1}^N \tilde{\beta}_{i,k}}. \quad (14)$$

The key difference between $\tilde{\beta}$ and β lies in the normalization applied to the latter. Specifically, β is normalized per time series, meaning that $\beta_{i,j}$ represents the proportional impact of time series j on time series i . This effectively quantifies the relative influence among time series. In contrast, $\tilde{\beta}$ is simply the aggregate of the α coefficients across all lags and does not provide insight into how the influence is distributed among the different time series.

Using the β coefficients, we can determine which time series are the key drivers behind each series in the system. Although the absolute value in the equation causes a loss of the interaction sign, the magnitude of the impact of each time series on another remains clear. Moreover, β values are intuitive and can be easily understood by a broad audience, not just domain experts or machine learning practitioners. Higher β values indicate stronger influence, while lower β values suggest weaker or negligible influence.

In addition, if the goal is to understand how the data is generated, i.e., to uncover the underlying equations governing the MTS system, we can refer back to the α coefficients. These coefficients provide a direct way to reconstruct the generating equations. Ultimately, DCIts is not only used to

predict the next step in the time series but also to decipher the equations driving the data. By analyzing both the α and β coefficients, we gain a deeper understanding of the system’s dynamics and structure.

Algorithm 1 Extracting Interpretability from Multivariate Time Series

Require: Windowed sample set Q

Require: Loss function \mathcal{L}

Split the sample set Q into training set Q_{train} , validation set Q_{val} , and test set Q_{test}

Shuffle the training set Q_{train}

Train the model M_{DCIIts} on Q_{train}

Evaluate the model on Q_{val} using \mathcal{L}

if validation loss does not improve for a predefined number of iterations
then

Stop training early

 ▷ Early stopping based on validation performance

end if

for each $Q_{t,\text{test}}$ in Q_{test} **do**

 Perform inference with the trained model M_{DCIIts} on $Q_{t,\text{test}}$

 Compute the $F_{t,\text{test}}$ and $C_{t,\text{test}}$ matrices for $Q_{t,\text{test}}$

 Calculate the transition tensor $\alpha_{t,\text{test}}$ as $\alpha_{t,\text{test}} = F_{t,\text{test}} \circ C_{t,\text{test}}$

end for

We opted to train the model on a forecasting task, under the conviction that this approach, as opposed to direct optimization for interpretability, fosters more genuine and causally interpretable insights. Typically, models and methods that impose excessive structure on anticipated interpretability can distort or entirely overlook it. Our approach minimally insists on linear interpretability, and then adds higher order terms as necessary, aligning with conventional modeling practices in physics. This choice is driven by several considerations. We contend that designing the model architecture with the forecasting task in mind, not only enhances the model’s predictive capability, but also ensures that the approximation closely mirrors the underlying equations generating the data. This alignment is crucial, as it allows the model to generate interpretability concurrently with forecasting. This means the model is equipped to recognize if different equations govern the data based on specific input values. Our aspiration is for this model to be universally applicable (unconstrained by data type), accurate (boasting robust predic-

tive power), and reliable (providing accurate interpretability) by enabling it to approximate the transition tensor effectively.

2.3. Optimal Window Size

A method for selecting the optimal window size for a multivariate time series (MTS) of size N within the DCIts framework employs a systematic evaluation process. This process can take two approaches.

First, one iteratively tests various window configurations within a predefined range by leveraging a loss function. For each configuration, the model is trained R times, and the loss on the test set is computed for each iteration. The average of these R loss values is used to evaluate the performance of each configuration, ultimately identifying the optimal window size, L_o , that minimizes the loss.

Second, since DCIts demonstrates robustness even when window sizes larger than the optimal value is selected, one can set a relatively large L_{\max} , run Algorithm 1 R times, and then look for the largest statistically significant lag in α . This characteristic is validated through experiments on benchmark datasets, as detailed in subsequent sections.

2.4. Higher order approximations

Until now we only discussed DCIts with the linear term, i.e. final output was a linear approximation of dynamics. In this section, we extend DCIts to include bias and higher order terms. The architecture of extended DCIts is shown in Figure 3.

In this section, we denote \mathbf{Q}_t as $\mathbf{q} = \mathbf{Q}_t$ for readability. To incorporate both higher-order terms and a bias term, we define a product operation on a sequence of tensors $\mathbf{q}^{(k)}$, allowing us to generalize the element-wise product. Specifically, we define:

$$\bigcirc_{k=0}^p \mathbf{q}^{(k)} = \begin{cases} \mathbf{I}, & \text{if } p = 0, \\ \mathbf{q}^{(1)} \circ \mathbf{q}^{(2)} \circ \dots \circ \mathbf{q}^{(p)}, & \text{if } p \geq 1, \end{cases}$$

where \mathbf{I} is the $n \times n$ identity matrix, representing the bias term when $p = 0$. This setup allows us to include the bias term within the same framework as higher-order interactions. Note that, due to the flexibility of framework one can introduce more complex bias terms incorporating influence of other series at different lags, but for now we opted for the simplest one. The transition equation with this formulation is given by:

$$X_{n,t+1} = \sum_{p=0}^P \sum_{i=1}^N \sum_{j=1}^L \left((\mathbf{C}_p \circ \mathbf{F}_p) \diamond \bigcirc_{k=0}^p \mathbf{q}^{(k)} \right)_{n,i,j}. \quad (15)$$

Here:

- For $p = 0$, the product $\bigcirc_{k=0}^p \mathbf{q}^{(k)} = \mathbf{I}$ introduces the bias term b_n , captured by $(\mathbf{C}_0 \circ \mathbf{F}_0)$.
- For $p \geq 1$, the term $\bigcirc_{k=0}^p \mathbf{q}^{(k)}$ represents the interaction of the lagged values $\mathbf{q}^{(1)}, \mathbf{q}^{(2)}, \dots, \mathbf{q}^{(p)}$.

This formulation allows DCITs to approximate the interactions between time series at various lags and the constant bias term for each series n in a unified, interpretable framework.

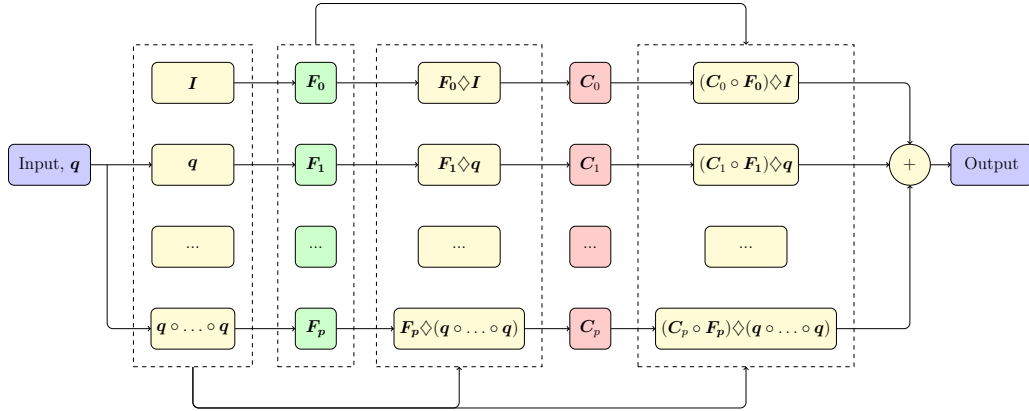


Figure 3: The architecture of the extended DCITs model incorporates bias and higher-order terms by adding new, parallel Focuser and Modeler modules. All Modeler modules, including all multiplications, utilize the Focuser's input and output.

The notation for the α , $\tilde{\beta}$, and β coefficients is adjusted to $\alpha^{(p)}$, $\tilde{\beta}^{(p)}$, and $\beta^{(p)}$ to reflect interpretability for a specific order. $\alpha^{(p)}$ for the p -term is generally expressed as:

$$\alpha^{(p)} = \mathbf{C}^{(p)} \circ \mathbf{F}^{(p)}.$$

If we use notation as α , $\tilde{\beta}$, and β we assume $p = 1$.

3. Assessing Model Performance and Interpretability Accuracy

This section examines the interpretability accuracy and forecasting performance of the DCIts architecture. Initially, the focus is on forecasting performance; then, the impact of different generating processes for test data on model performance and interpretability is examined. The general code is written in Python and the DCIts neural network is implemented using PyTorch. The complete code, along with examples, is accessible on GitHub [27]. The training utilizes the Adam optimizer, featuring a learning rate of 10^{-3} , and a batch size of 64 unless stated otherwise. When optimizing the hyperparameters of a model (e.g., learning rate, batch size), it is essential to be mindful of potential overfitting to the hyperparameters. As the optimization process is driven by a loss function focused primarily on enhancing predictive performance, there is a risk of overfitting to this objective while neglecting interpretability. All model training and inference tasks were performed on an Intel® Xeon® Gold 6142 CPU with 252 GB of RAM and an NVIDIA RTX A4000 GPU.

The benchmarking datasets used in this study were sourced from Barić et al. [2], with minor typographical errors corrected to align with the generating code as described in the reference. Additionally, the generating process for Dataset 8 was adjusted with the first time series now containing the switching process. Full details of the datasets utilized in this work are provided in Appendix A for reference. Furthermore, the performance of the DCIts model is benchmarked against the IMV-LSTM model, which was identified as the top-performing model by the authors in [2].

3.1. Quantitative analysis

We examine the forecasting error, quantified by the Mean Square Error (MSE), across the eight datasets utilized in Barić et al. [2]. A comparative analysis of the DCIts and IMV-LSTM models' performance on these datasets is conducted. The stability of the errors over multiple iterations on the same dataset is analyzed, and an exploration of how error rates fluctuate in response to variations in data generation parameters is undertaken.

In Table 1, we compare the average Mean Squared Error (MSE) for two architectures, DCIts and IMV-LSTM. The average errors are comparable, displaying similar error patterns across all datasets. Specifically, DCIts shows equal or slightly better performance on all datasets, regardless of their complexity, which aligns with its design as it approximates generating process.

The optimal time window was set to 10 so that we can directly compare our results to IMV-LSTM.

This distinction in performance is also reflected in the models’ stability, analyzed in Figure 4. Here, the standard deviation of the experiment error, divided by the average experiment error, illustrates the stability of each model. Circles represent DCIts, and squares represent IMV-LSTM. Both models exhibit comparable performance, with slight differences in stability. Notably, DCIts demonstrates better performance and stability on all datasets. In Dataset 8, IMV-LSTM appears to exhibit greater stability; however, this is due to the fact that the results for DCIts are an order of magnitude smaller, making minor variations more prominent in relative terms.

All Datasets 1–8 were generated following the process used in [2]. Points for each time series were first sampled from the normal distribution $\mathcal{N}(\mu = 0, \sigma^2 = 1)$, setting the initial values for each time series, which were then extended by generating values at each time step according to the model described in Appendix A. Values were generated sequentially, and Gaussian noise ϵ_t was introduced by sampling a value p from a random uniform distribution within the range $[0, 1)$, $p \sim \text{Uniform}(0, 1)$:

$$\epsilon_t = \begin{cases} \mathcal{N}(\mu = 0, \sigma^2 = \sigma_{noise}^2), & \text{if } p < f, \\ 0, & \text{else,} \end{cases}$$

f represents noise frequency. In all generated series f is fixed to 0.3, and σ_{noise}^2 to 0.1 (if not otherwise specified). The stability of prediction performance is evaluated by the ratio of the standard deviation to the mean of the Mean Squared Error (MSE); lower values indicate greater stability.

Dataset	DCITs	IMV-LSTM
1	$(2.98 \pm 0.01) \times 10^{-3}$	$(2.91 \pm 0.01) \times 10^{-3}$
2	$(7.58 \pm 0.02) \times 10^{-4}$	$(1.81 \pm 0.19) \times 10^{-3}$
3	$(6.17 \pm 0.15) \times 10^{-5}$	$(1.25 \pm 0.06) \times 10^{-4}$
4	$(1.23 \pm 0.01) \times 10^{-4}$	$(2.38 \pm 0.05) \times 10^{-4}$
5	$(1.25 \pm 0.01) \times 10^{-3}$	$(1.38 \pm 0.03) \times 10^{-3}$
6	$(1.27 \pm 0.02) \times 10^{-3}$	$(1.43 \pm 0.06) \times 10^{-3}$
7	$(3.10 \pm 0.03) \times 10^{-3}$	$(5.14 \pm 0.64) \times 10^{-3}$
8	$(2.55 \pm 0.49) \times 10^{-2}$	$(2.58 \pm 0.02) \times 10^{-1}$

Table 1: The model prediction performance is evaluated across all datasets, with the average experiment Mean Squared Error (MSE) for each model reported as a score. DCITs demonstrates similar or better overall performance to IMV-LSTM.

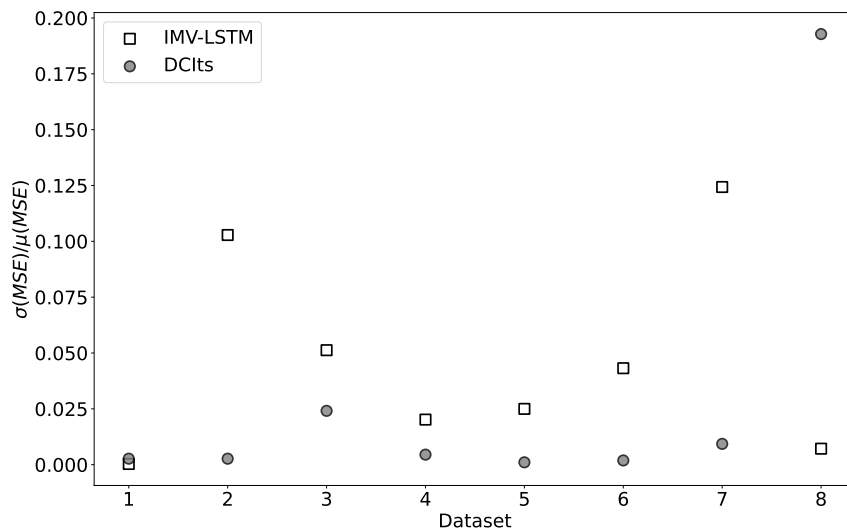


Figure 4: The stability of prediction performance by dataset is assessed by plotting the standard deviation of the Mean Squared Error (MSE) divided by the mean MSE value on the y-axis. The x-axis represents the index of each dataset.

The stability of prediction performance was performed on Dataset 2 with parameters ranging as follows:

- Noise frequency f varied from 0 to 1 with a step of 0.05

- Number of time series N ranged from 3 to 19 with a step of 2
- Noise amount: σ_{noise}^2 —values are: 0.01, 0.05, 0.1, 0.2, 0.5, 1, 2, 3, and 5.

Figure 5 provides two important insights into the models’ performance. On the left side of the figure, the focus is on how prediction stability varies with changes in noise frequency, represented by f . DCITs shows resilience against fluctuations in noise levels, only exhibiting a small increase in instability at very high frequencies. In contrast, IMV-LSTM displays a marked rise in instability for $f > 0.4$. The right panel of the figure analyzes the impact of varying the number of time series, N , on prediction stability. In this context, DCITs consistently outperforms IMV-LSTM, showcasing superior stability across diverse testing conditions. Additionally, both models demonstrate similar behavior and achieve comparable performance for noise levels $\sigma_{noise}^2 \leq 1$. However, for $\sigma_{noise}^2 > 1$, DCITs achieves a significantly lower mean squared error (MSE), outperforming IMV-LSTM by an order of magnitude.

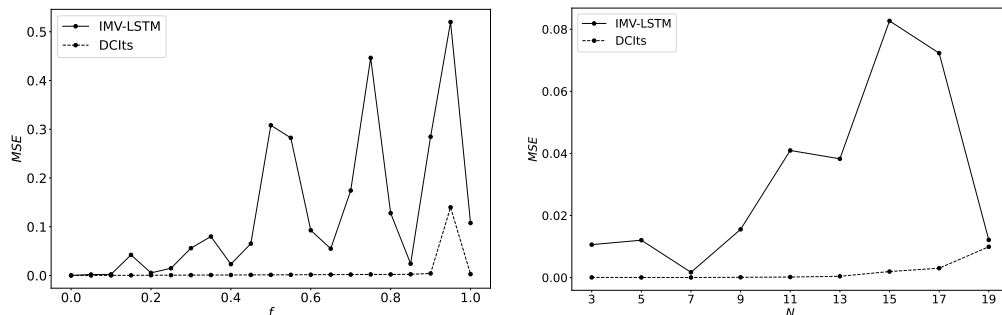


Figure 5: The left figure illustrates how the stability of prediction performance for a specific model varies with noise frequency f for Dataset 2. DCITs is more resilient to changes in noise frequency, with increasing instability only at the highest noise frequencies. The right figure examines the stability of prediction performance as the number of time series N increases in Dataset 2. Here, DCITs again demonstrates greater stability compared to IMV-LSTM across all values of N .

DCITs exhibits similar and more stable predictive power compared to IMV-LSTM. As will be discussed in the upcoming section, it also offers significantly more reliable interpretability. The comparison of these two models using the Performance-Explainability Framework is illustrated in Figure 6, which integrates six key evaluation components: performance, comprehensibility, granularity, information, faithfulness, and type of user. Performance:

This component evaluates the efficacy of deep learning models by comparing their performance in specific applications and settings to the state-of-the-art model. **Comprehensibility:** This aspect relates to how well users can understand the model’s operations and the predictions it generates. **Granularity:** This measures the level at which the model provides explainability, whether local (pertaining to individual predictions) or global (across the model’s overall behavior). **Information:** This details the type of information the model conveys to the user. **Faithfulness:** This evaluates the reliability of the explanations provided by the model concerning its predictions. **User:** This category assesses the accessibility of the explanations, specifically how much prior knowledge is required for users to understand the model’s explanations.

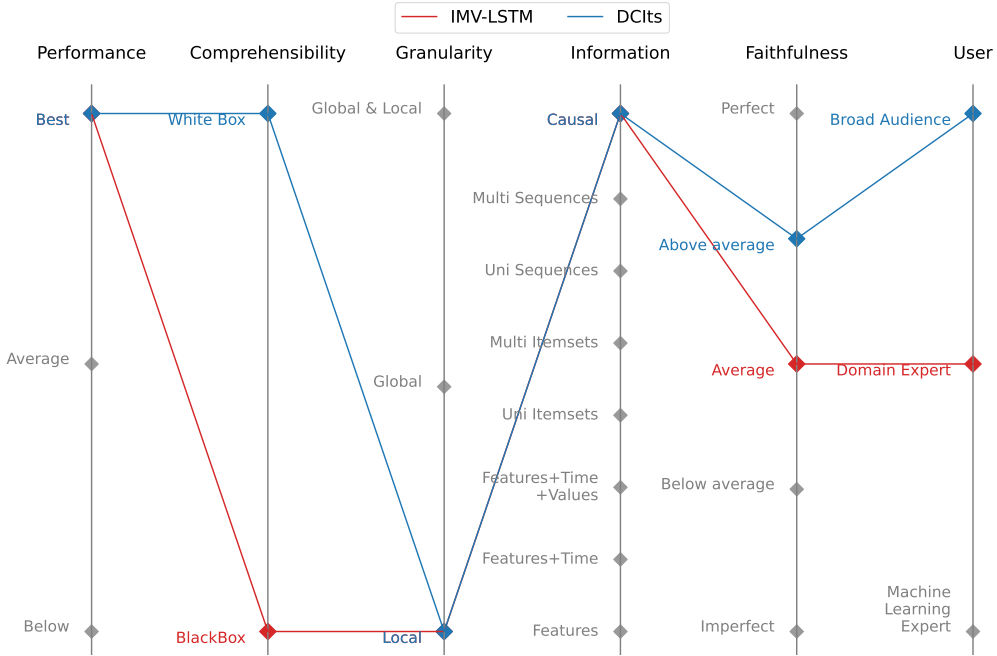


Figure 6: Parallel coordinates plot of evaluated models within Performance-Explainability Framework

3.2. Optimal window size examples

We present optimal window size results for Datasets 2, 4, and 7, with $R = 5$, $L_{\min} = 3$, $L_{\max} = 12$, and $L_{\text{step}} = 1$. We expect to achieve the

best results for $L_o = 7$ for Dataset 2, $L_o = 9$ for Dataset 4, and $L_o = 5$ for Dataset 7. Figure 7 shows the normalized test loss (using MAE as loss function) by window size, and we can see that, for optimal window sizes we have significant drop in loss function and low variability of the loss function in positions that correspond to the optimal window.

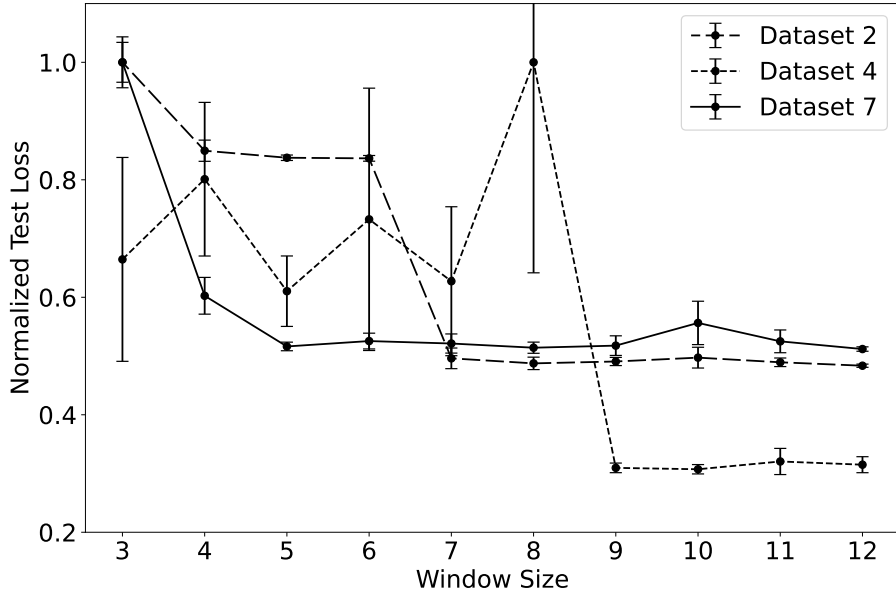


Figure 7: Impact of window size on loss. On the x-axis we plot window size, on the y-axis, we plot normalized loss on the test set. Optimal window sizes for Datasets 2, 4, and 7, are 7, 9, and 5, respectively. We can see that, for optimal window sizes we have drop in loss function and low variability of the loss function.

As previously noted, DCIts demonstrates robustness in accurately identifying interactions even when a window size larger than optimal is selected. Figure 8 presents the statistically significant $\alpha_{1,j,l}$ values for Dataset 7 with a window size of $L = 7$ and $R = 5$ runs. Specifically, the mean α coefficients were computed on the test set across five runs, and only those elements that were statistically significantly different from zero were retained. Notably, all $\alpha_{i,j,l}$ elements with $l > 5$ were equal to zero.

3.3. Qualitative analysis

Next, we examine the interpretability and faithfulness of the results produced by the DCIts architecture. Before presenting the results for the bench-

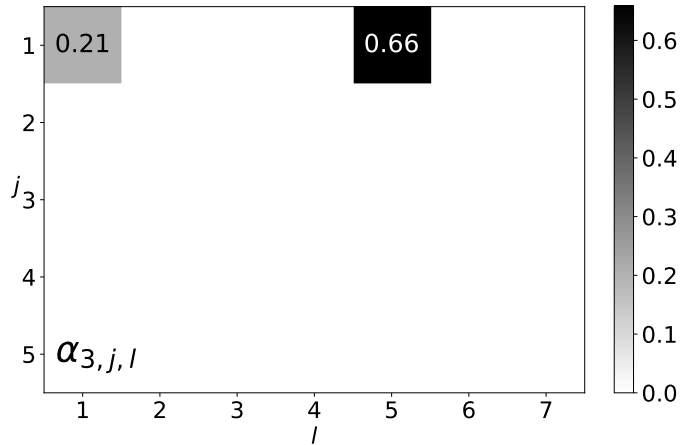


Figure 8: Statistically significant $\alpha_{1,j,l}$ values for Dataset 7 with $L = 7$ and $R = 5$. All $\alpha_{1,j,l}$ elements with $l > 5$ are correctly identified as zero.

marking datasets, we first demonstrate the strength of the DCIts architecture using a simple second-order vector autoregressive (VAR(2)) process:

$$\mathbf{Y}_t = \mathbf{A}_1 \mathbf{Y}_{t-1} + \mathbf{A}_2 \mathbf{Y}_{t-2} + \boldsymbol{\epsilon}_t$$

where $\mathbf{Y}_t^T = (Y_{1,t}, Y_{2,t}, Y_{3,t})$, and the lag-1 and lag-2 matrices \mathbf{A}_1 and \mathbf{A}_2 are of dimension 3×3 . The noise terms $\boldsymbol{\epsilon}_t$ are sampled from a Gaussian distribution $\mathcal{N}(0, 0.2)$. The VAR(2) process serves as an ideal starting point to validate the interpretability and performance of the DCIts model. We can observe its ability to accurately identify underlying interactions and dependencies between variables.

The identified optimal window size is $L_o = 2$. Using the $\boldsymbol{\alpha}$ coefficients, we can easily reconstruct the coefficient matrices used in generating the time series. Specifically, we select the $\boldsymbol{\alpha}$ coefficients corresponding to lag-1 and lag-2. For the VAR(2) process, the matrices \mathbf{A}_1 and \mathbf{A}_2 reconstructed by DCIts are presented below. The ground truth values are shown in bold font, and beneath each ground truth value, we present the DCIts reconstruction in the form of the mean value \pm standard deviation of the $\alpha_{i,j,l}$ coefficients. The mean value is rounded to two decimal places for presentation purposes,

but results show that significant digits are all zero after second decimal place.

$$A_1 = \begin{pmatrix} \mathbf{0.40} & \mathbf{0.10} & \mathbf{0.05} \\ 0.40 \pm 10^{-5} & 0.10 \pm 10^{-4} & 0.05 \pm 7 \cdot 10^{-5} \\ \mathbf{0.10} & \mathbf{0.40} & \mathbf{0.10} \\ 0.10 \pm 2 \cdot 10^{-5} & 0.40 \pm 2 \cdot 10^{-4} & 0.10 \pm 10^{-4} \\ \mathbf{0.05} & \mathbf{0.02} & \mathbf{0.40} \\ 0.05 \pm 5 \cdot 10^{-6} & 0.02 \pm 5 \cdot 10^{-5} & 0.40 \pm 5 \cdot 10^{-5} \end{pmatrix}$$

$$A_2 = \begin{pmatrix} \mathbf{0.20} & \mathbf{0.05} & \mathbf{0.02} \\ 0.20 \pm 10^{-4} & 0.05 \pm 10^{-5} & 0.02 \pm 4 \cdot 10^{-6} \\ \mathbf{0.05} & \mathbf{0.20} & \mathbf{0.05} \\ 0.05 \pm 10^{-5} & 0.20 \pm 2 \cdot 10^{-4} & 0.05 \pm 5 \cdot 10^{-6} \\ \mathbf{0.02} & \mathbf{0.05} & \mathbf{0.20} \\ 0.02 \pm 5 \cdot 10^{-5} & 0.05 \pm 7 \cdot 10^{-5} & 0.20 \pm 10^{-4} \end{pmatrix}$$

Our discussion primarily focuses on the interpretability provided by DCIts for the datasets listed in Appendix A. The optimal window size has been thoroughly discussed in Section 3.2, and we employ the optimal time window for the remaining benchmarking datasets. All presented results for α and β coefficients are obtained from mean values across five runs using MAE as the loss function unless stated otherwise. This approach assesses the stability of the results, as we utilize a fixed random seed to generate the time series.

3.3.1. Autoregressive Datasets

We will start the analysis of the interpretability and faithfulness of the DCIts architecture on benchmarking datasets with Dataset 2. For brevity, detailed results for Dataset 1 are omitted here. In Dataset 1, each time series is represented by a constant and DCIts accurately identifies time series generating process. The corresponding results can be found in the examples folder of [27]. Dataset 2 consists of five autoregressive time series that do not interact with each other. In the right panel of Figure 9, the β coefficients estimated by DCIts are shown. Since the dataset is composed solely of autoregressive time series, the ground truth for the β coefficients corresponds to the identity matrix, as determined by the generating α values. As illustrated in the left panel of Figure 9, the model successfully captures the underlying dynamics of Dataset 2, producing correct interpretability with high confidence. The mean values of the β diagonal elements across all samples range from 0.9979 to 0.9994, with standard deviations between 10^{-4} and $3 \cdot 10^{-4}$, the ground truth being 1. In contrast, the mean values of the off-diagonal

elements range from 10^{-4} to $7 \cdot 10^{-4}$, with standard deviations between 10^{-4} and 10^{-3} , the ground truth is 0.

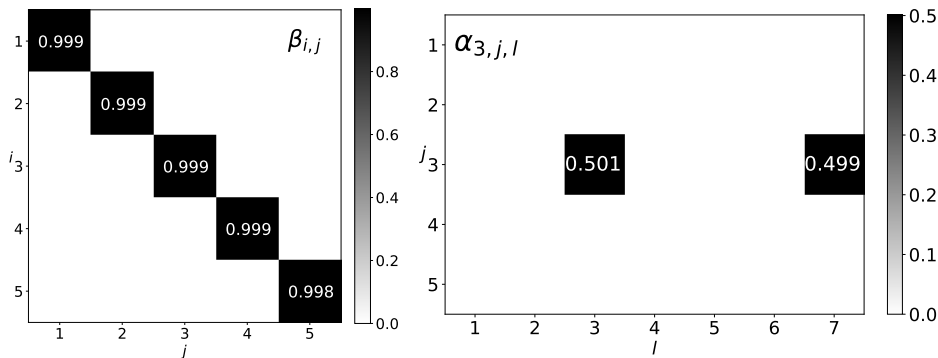


Figure 9: In the left panel, the β coefficients estimated by DCIts for Dataset 2 are shown. The y-axis corresponds to the target series index, and the x-axis corresponds to the source time series. Since this dataset consists solely of autoregressive time series with no interactions between them, the ground truth β values correspond to the identity matrix, with nonzero values only on the diagonal. The model correctly identifies these dynamics, producing near-zero off-diagonal and diagonal elements close to one. In the right panel, α coefficients are shown for a single time series $X_{3,t}$. The y-axis corresponds to the time series index (j), and the x-axis corresponds to the lag (l) of $\alpha_{3,j,l}$ coefficient. Lags 3 and 7 are the key contributors, closely matching the ground truth values of 0.5. All other $\alpha_{3,j,l}$ values are significantly smaller.

In the right panel of Figure 9, the $\alpha_{3,j,l}$ coefficients are displayed for a single time series $X_{3,t}$ in Dataset 2 (a similar pattern is observed for all other time series in this dataset). The lags 3 and 7 are the key contributors to generating the next step in the time series. DCIts correctly identifies that Dataset 2 is an autoregressive problem, with no interaction between the time series; that is, time series $X_{3,t}$ is generated solely by $X_{3,t}$. DCIts also accurately recognized the most significant lags, with the $\alpha_{3,3,l}$ coefficients for lags 3 and 7 ($\alpha_{3,3,3}^{\text{gt}} = \alpha_{3,3,7}^{\text{gt}} = 0.5$) being $\alpha_{3,3,3} = (0.4992 \pm 0.0007)$ and $\alpha_{3,3,7} = (0.5010 \pm 0.0008)$, while all other α values are significantly smaller and/or statistically not significant. Additionally, the α coefficients exhibit low variability across all samples.

A similar behavior is observed in Dataset 3 when using the linear version of DCIts, even though Dataset 3 is generated by a nonlinear process, which makes it more suitable for analysis with higher-order terms in DCIts.

3.3.2. Datasets with cross correlation

Datasets 4, 5, and 6 are used to assess the performance of DCITs when cross-correlations are present. In our previous work [2], these datasets presented a significant challenge to benchmarked interpretable models.

Dataset 4 is characterized by the presence of only cross-correlations, with no autocorrelation. When analyzing the mean and standard deviation of the α coefficients obtained for Dataset 4 using the MAE loss function in Figure 10, it is evident that Algorithm 1 successfully identified values corresponding to the ground truth. Furthermore, Algorithm 1 provides a highly stable interpretation across all samples, accurately identifying the correct interactions and lags. Specifically, values are $\alpha_{1,2,2} = (0.396 \pm 0.004)$, $\alpha_{1,2,2}^{\text{gt}} = 2/5$, $\alpha_{1,2,5} = (0.197 \pm 0.005)$, $\alpha_{1,2,5}^{\text{gt}} = 1/5$, $\alpha_{1,2,9} = (0.398 \pm 0.004)$, $\alpha_{1,2,9}^{\text{gt}} = 2/5$, $\alpha_{2,1,2} = (0.399 \pm 0.006)$, $\alpha_{2,1,2}^{\text{gt}} = 2/5$, $\alpha_{2,1,5} = (0.196 \pm 0.004)$, $\alpha_{2,1,5}^{\text{gt}} = 1/5$, $\alpha_{2,1,9} = (0.397 \pm 0.008)$, $\alpha_{2,1,9}^{\text{gt}} = 2/5$. As we mentioned, interpretability is robust on the choice of the loss, function, but in the case of Dataset 4, the MAE loss function behaves better with respect to MSE. When MSE is used as a loss function the validation loss does not follow a smooth trend and exhibits large oscillations.

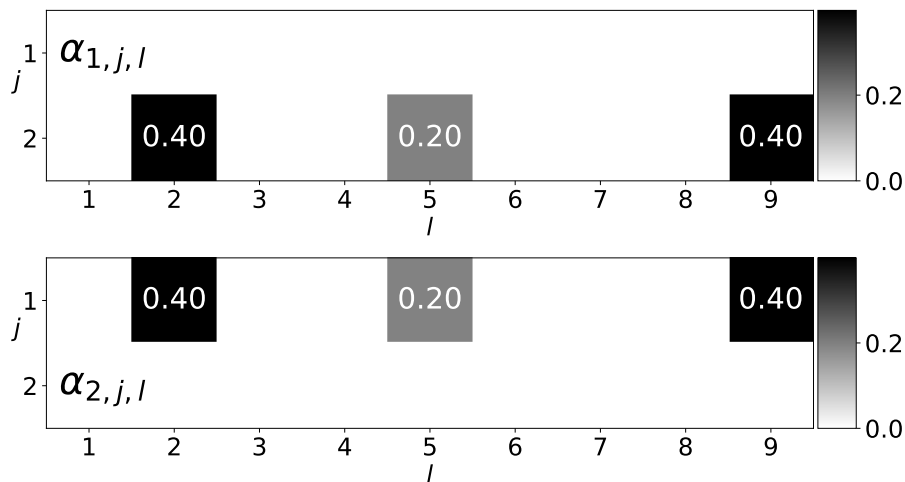


Figure 10: Mean α values for Dataset 4, obtained using MAE as the loss functions by Algorithm 1 match ground truth values. The y-axis corresponds to the source time series index (j), and the x-axis represents the time lag (l).

In Datasets 5 and 6, each time series is generated based on the first time series, $X_{1,t}$. Since Dataset 6 is more suited for the higher-order version of

DCIts, the focus here remains on Dataset 5. In Figure 11, we present the β , and $\alpha_{4,j,l}$ values estimated by DCIts using MAE as the loss function for Dataset 5.

The ground truth for Dataset 5 is given by $\beta_{i,1} = 1$ for all i , with all other β values being zero. The mean values of $\beta_{i,1}$ across all samples fall within (0.98, 0.99), with standard deviations ranging from 0.01 to 0.03. All other β values equal zero.

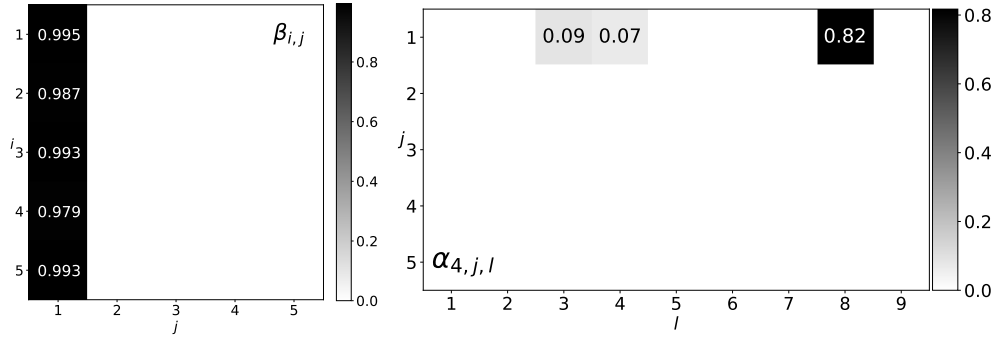


Figure 11: Mean β values estimated by DCIts using MSE (left panel) and $\alpha_{4,j,l}$ values (right panel) for Dataset 5. The ground truth is given by $\beta_{i,1} = 1$ for all i , with all other β values being zero. Each time series in this dataset depends solely on $X_{1,t}$, and DCIts correctly identified $X_{1,t}$ as a source for all time series. DCIts correctly identified important lags with relatively smaller impact in $\alpha_{4,j,l}$.

Analyzing interpretability at the single time series level for Dataset 5 reveals that DCIts, utilizing the MAE as the loss function, accurately identifies the most significant lags. For instance, in the case of $X_{5,t}$, the ground truth coefficients are $\alpha_{5,1,2}^{\text{gt}} = 1/3$, $\alpha_{5,1,5}^{\text{gt}} = 2/9$, and $\alpha_{5,1,8}^{\text{gt}} = 4/9$. The model successfully and with high confidence identified all significant lags, yielding $\alpha_{5,1,2} = (0.336 \pm 0.003)$, $\alpha_{5,1,5} = (0.222 \pm 0.004)$, and $\alpha_{5,1,8} = (0.43 \pm 0.01)$. All other $\alpha_{5,j,l}$ values were correctly estimated as nonsignificant.

Similarly, for $X_{4,t}$, the ground truth coefficients are $\alpha_{4,1,3}^{\text{gt}} = 1/10$, $\alpha_{4,1,4}^{\text{gt}} = 1/10$, and $\alpha_{4,1,8}^{\text{gt}} = 4/5$. The model again successfully and with high confidence identified all significant lags, resulting in $\alpha_{4,1,3} = (0.09 \pm 0.01)$, $\alpha_{4,1,4} = (0.07 \pm 0.03)$, and $\alpha_{4,1,8} = (0.82 \pm 0.01)$. These results demonstrate DCIts's capability to accurately interpret important lags, even those with relatively smaller impacts.

3.3.3. High mixture of behaviours

With Dataset 7, we evaluate the performance of DCIts in scenarios where bias and a mixture of different dynamics exist between time series in the generating process, including autoregressive processes and cross-correlations that may be positive or negative. In this dataset, the time series $X_{2,t}$ and $X_{4,t}$ include constant terms in their generating processes, with ground-truth values $b_2^{\text{gt}} = 1$ and $b_4^{\text{gt}} = 1$. Using both bias and linear terms ($p = 0$ and 1), DCIts accurately identified the bias values as $b_2 = (0.89 \pm 0.07)$ and $b_4 = (0.97 \pm 0.02)$.

Figure 12 presents the results for the $\alpha_{2,j,l}$ and $\alpha_{4,j,l}$ coefficients: $\alpha_{2,1,2}^{\text{gt}} = -1$, $\alpha_{2,1,2} = (-0.94 \pm 0.04)$; $\alpha_{4,3,4}^{\text{gt}} = -2/7 \approx -0.286$, $\alpha_{4,3,4} = (-0.27 \pm 0.02)$; $\alpha_{4,5,1}^{\text{gt}} = -5/7 \approx -0.714$, $\alpha_{4,5,1} = (-0.71 \pm 0.01)$. DCIts successfully identified the correct lags and accurately determined the sign of the interactions.

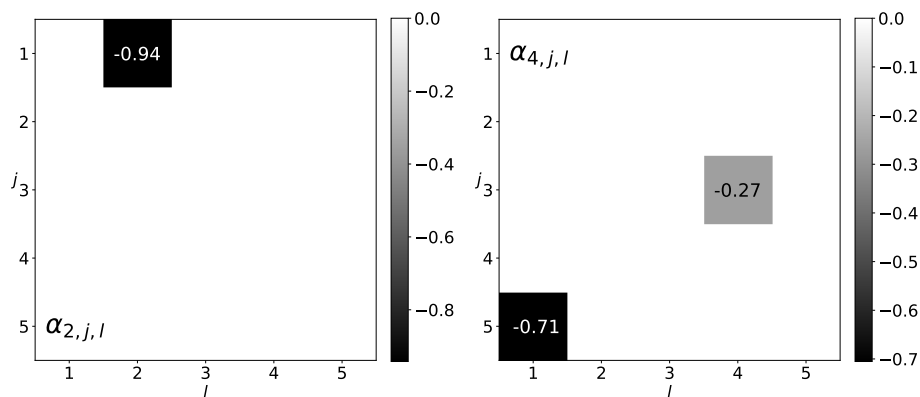


Figure 12: The mean values of $\alpha_{2,j,l}$ (left panel) and $\alpha_{4,j,l}$ (right panel) for Dataset 7. The y-axis corresponds to the source time series index (j), and the x-axis represents the time lag (l). DCIts not only identifies the important time series and lags but can also detect the correct sign and strength of the interaction. For Dataset 7 DCIts accurately identified the source time series with the correct lag, sign, and magnitude of interaction.

3.3.4. Time series with multiple dynamics

Dataset 8 is an example of a dataset that exhibits two distinct dynamics, with the active dynamic determined by the value of $X_{1,t-5}$. This dataset allows us to test whether DCIts can detect the presence of two different dynamics.

The time series $X_{1,t}$ alternates between two levels, $b_{\text{low}} = 0.2$ and $b_{\text{high}} = 0.7$, with persistence durations drawn from a normal distribution. Formally,

$X_{1,t}$ is defined as:

$$X_{1,t} = b_t + \epsilon_{1,t}.$$

The b_t switches between b_{low} and b_{high} based on a persistence duration, P , which is randomly sampled from a truncated normal distribution:

$$P \sim \max(10, \mathcal{N}(\mu_P, \sigma_P)),$$

where $\mu_P = 50$ is the mean persistence duration, and $\sigma_P = 30$ is the standard deviation. The truncation ensures a minimum persistence duration of 10 time steps. Gaussian noise, $\epsilon_{1,t}$, is added to the $X_{1,t}$ similarly to other benchmarking datasets.

The following condition determines the switching mechanism:

$$b_t = \begin{cases} b_{\text{high}}, & \text{if } b_{t-1} = b_{\text{low}} \text{ and } t - t_{\text{last switch}} \geq P, \\ b_{\text{low}}, & \text{if } b_{t-1} = b_{\text{high}} \text{ and } t - t_{\text{last switch}} \geq P, \end{cases}$$

where $t_{\text{last switch}}$ denotes the time step when the most recent level switch occurred.

Before analyzing whether DCIts can identify the changing dynamics in the dataset, we first examine the results for $X_{4,t}$ to assess if the model can correctly capture the generating process for time series with fixed dynamics. $\alpha_{4,j,l}$ values are $\alpha_{4,4,1} = (0.50001 \pm 0.0001)$, and $\alpha_{4,4,4} = (0.40001 \pm 0.0003)$, for $X_{1,t-5} \leq 0.5$, and $\alpha_{4,4,1} = (0.4999 \pm 0.0001)$, and $\alpha_{4,4,4} = (0.4002 \pm 0.0006)$, for $X_{1,t-5} > 0.5$. The ground truth for are 1/2, and 2/5, respectively. So in the case of fixed dynamics DCIts reconstructed the generating process successfully.

Results for $X_{1,t}$ are the only instance where DCIts deviates from perfect faithfulness. For $X_{1,t-5} \leq 0.5$, it correctly determines that there is bias present with $b_1 = (0.196 \pm 0.004)$ (ground truth is 0.2), and the only non-zero $\alpha_{1,j,l}$ element is $\alpha_{1,1,1} = (0.06 \pm 0.02)$. The ground truth for all $\alpha_{1,j,l}$ values is zero. Therefore, we can conclude that the model correctly deciphered the dynamics. For $X_{1,t-5} > 0.5$, DCIts does not detect the shift in bias, remaining fixed at $b_1 = (0.196 \pm 0.004)$ (ground truth 0.7), and instead utilizes $\alpha_{1,1,1} = (0.49 \pm 0.04)$. We attempted to modify the structure of the $p = 0$ focuser so that the input is Q_{t-1} rather than I , but this did not alter the outcome.

According to the generating process for Dataset 8, $\alpha_{2,1,5}$ is expected to be $\alpha_{2,1,5}^{\text{gt}} = 4/5$ when $X_{1,t-5} > 0.5$, and it should be zero when $X_{1,t-5} \leq 0.5$.

Conversely, for $\alpha_{2,4,2}$, $\alpha_{2,4,2}^{\text{gt}}$ is expected to be zero when $X_{1,t-5} > 0.5$, and $2/3$ when $X_{1,t-5} \leq 0.5$. In Figure 13, we plot histograms for the values of $\alpha_{2,1,5}$ and $\alpha_{2,4,2}$ based on the value of $X_{1,t-5}$. We observe the bimodal distribution in both histograms indicating that DCIts successfully detected the two different dynamics in this dataset, with $\alpha_{2,4,2} = (0.6663 \pm 0.0005)$ and $\alpha_{2,1,5} = (0.796 \pm 0.005)$. The same is true for $\alpha_{3,4,4} = (0.800 \pm 0.001)$ and $\alpha_{3,1,4} = (0.665 \pm 0.002)$. For $X_{2,t}$ and $X_{3,t}$, DCIts again perfectly reconstructed the dynamics in this challenging switching case. Figure 14 shows

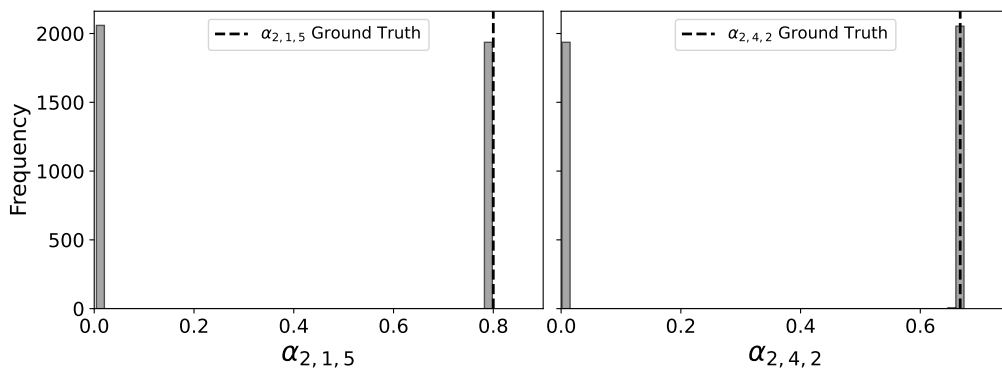


Figure 13: Histograms for $\alpha_{2,1,5}$ (left) and $\alpha_{2,4,2}$ (right). Both distributions are bimodal (elements are either close to zero or to ground truth), indicating that DCIts successfully detected the two different dynamics in this dataset.

$F_{2,j,l}$, i.e., the $p = 1$ focuser values for $X_{2,t}$. We see that this ability stems from the focuser identifying the correct time series and lag in generating dynamics, giving lower weights to the non-present generating elements in the $X_{1,t-5} \leq 0.5$ and $X_{1,t-5} > 0.5$ regimes. The final α values are fixed by the modeler \mathbf{C} .

3.4. Testing higher order DCIts

To analyze DCIts behavior with higher-order approximations, we utilize a process inspired by the Cubic map $X_t = aX_{t-1}^3 + (1-a)X_{t-1}$ with $a = 3.75$:

$$\begin{aligned}
 X_{1,t} &= (1-a)X_{1,t-3} + aX_{1,t-3}^3 + \epsilon_{1,t} \\
 X_{2,t} &= (1-a)X_{2,t-5} + aX_{2,t-5}^3 + \epsilon_{2,t} \\
 X_{3,t} &= \frac{1}{2}(X_{3,t-3} + X_{3,t-5}) + \epsilon_{3,t}.
 \end{aligned} \tag{16}$$

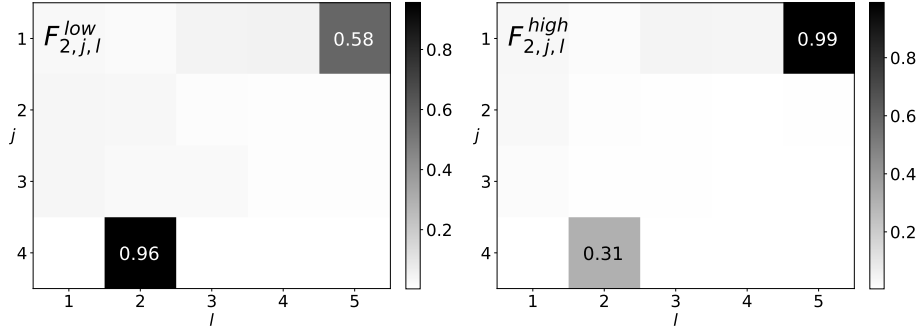


Figure 14: Mean focuser $F_{2,j,l}$ values for $X_{1,t-5} \leq 0.5$ (left panel) and $X_{1,t-5} > 0.5$ (right panel) from the DCIts model for Dataset 8. The y-axis corresponds to the source time series j , and the x-axis corresponds to the lag l . The focuser correctly identified the most important lags in both dynamics, giving lower weights to the non-present generating element.

In Figure 15, we plot the $\tilde{\beta}$ values for the linear and cubic terms of DCIts and compare them to the ground truth for the Cubic process, Equation (16). We use $\tilde{\beta}$ instead of β to emphasize that DCIts learned the practically exact coefficient values used during data generation. Furthermore, for $X_{3,t}$, DCIts correctly identified that only the linear term is present, i.e., the cubic term is zero for the last time series. When examining the sign of the linear $\alpha^{(1)}$ coefficients, we can see that DCIts learned that the linear term for the first two time series has a negative sign. We have the ground truth values $\alpha_{1,1,3}^{(1),\text{gt}} = \alpha_{2,2,5}^{(1),\text{gt}} = -2.75$. The DCIts results are $\alpha_{1,1,3}^{(1)} = (-2.749 \pm 0.04)$ and $\alpha_{2,2,5}^{(1)} = (-2.7501 \pm 0.0006)$. DCIts also correctly learned that there is no quadratic order present, i.e., all $\alpha^{(2)}$ values are zero.

4. Conclusion

In this paper, we introduced the Deep Convolutional Interpreter for Time Series, an interpretable deep learning model designed for multivariate time series forecasting. The architecture of DCIts prioritizes both predictive performance and interpretability, which is essential for understanding complex dynamic systems in various fields such as physics, finance, healthcare, and environmental monitoring. Through extensive experiments on synthetic and benchmark datasets, we demonstrated that DCIts effectively identifies the most relevant time series and lags (in the current case, ones that contribute

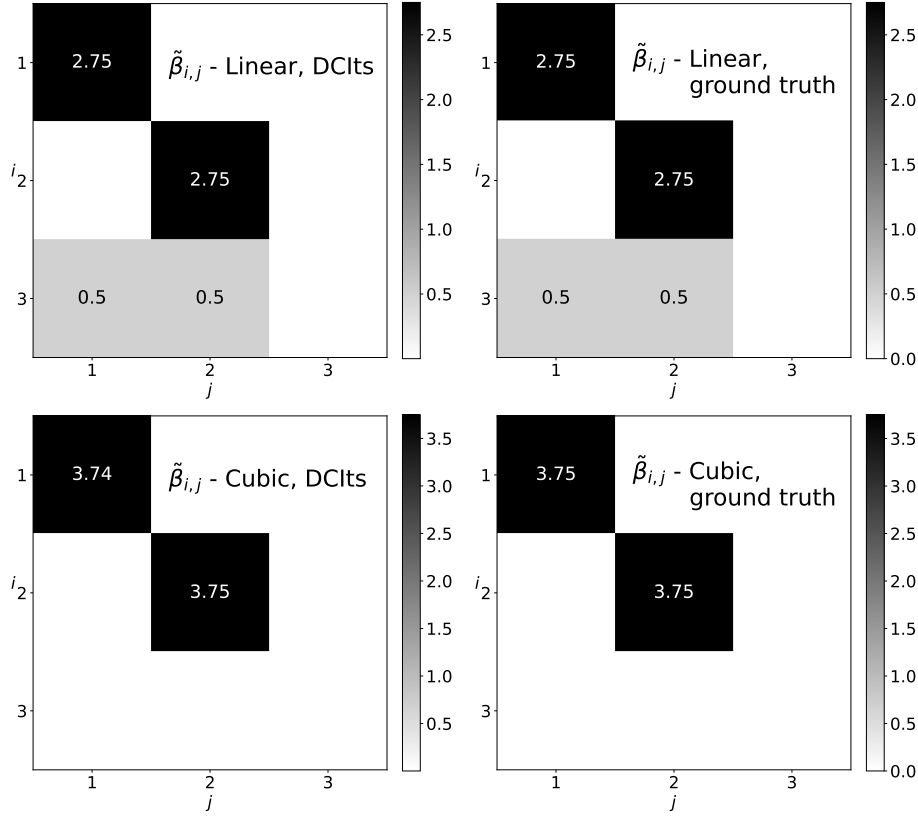


Figure 15: $\tilde{\beta}$ coefficients for linear and cubic terms learned by DCIts, and ground truth values for the Cubic process. DCIts learned correctly both linear and cubic terms, and it also learned that $X_{3,t}$ is just the linear combination of $X_{1,t}$ and $X_{2,t}$ which are both cubic maps.

to forecasting future values), providing intuitive and transparent explanations for its predictions. The model was able to reconstruct the underlying equations governing the time series, accurately capturing significant interactions and their corresponding lags. When applied to a standard second-order vector autoregressive (VAR(2)) process, DCIts accurately reconstructed the coefficient matrices used in generating the time series, with estimated coefficients closely matching the ground truth values. In datasets involving only autoregressive processes, such as Dataset 2, the model successfully identified that each time series depended solely on its own past values, correctly producing an identity matrix for the β coefficients.

When dealing with datasets containing cross-correlations, like Datasets 4

and 5, DCIts demonstrated robustness in capturing the underlying dynamics. The model correctly identified cross-series dependencies and was able to distinguish between autoregressive and cross-correlated relationships. Notably, these datasets also illustrated how to choose a loss function. In Dataset 7, which includes bias, and a mixture of behaviors with both positive and negative correlations, DCIts not only identified the significant interactions but also accurately determined the sign and magnitude of these interactions. Moreover, DCIts proved capable of detecting changing dynamics within a dataset. In Dataset 8, where the active dynamic depends on the value of a specific time series at a certain lag, the model effectively identified the presence of two different dynamics, accurately capturing the conditions under which each dynamic was active.

We presented the extension of DCIts to include higher-order approximations. By incorporating only cubic terms into the model architecture, DCIts showed that it can identify correct order of interactions and capture nonlinear dynamics that are prevalent in many real-world time series. In the case of the cubic process, DCIts learned both the linear and cubic terms correctly and identified that one of the time series was purely linear, while the others exhibited cubic behavior. This ability to discern and model nonlinear relationships enhances the versatility and applicability of DCIts to a broader range of dynamic systems.

While the DCIts model demonstrates promising results in both forecasting accuracy and interpretability, it is important to acknowledge certain limitations that may affect its performance and generalizability. These limitations provide valuable insights for future research and model refinement. As the model incorporates higher-order terms and processes larger windows of time series data, the computational complexity increases. This can impact the scalability of the model when applied to very large or high-frequency datasets. Optimizing the model’s architecture for computational efficiency, possibly through parallelization or approximation methods, could be an area of further development. While the model has shown strong performance on synthetic and benchmark datasets, real-world time series data often present additional challenges such as noise, missing values, and structural breaks. Extending the model’s capabilities to handle these issues will enhance its practical applicability. Incorporating data preprocessing steps, robustness checks, and validation on real-world datasets from various domains would be beneficial. Also, incorporating domain-specific knowledge into the model to guide the interpretability and potentially improve prediction accuracy. This

could involve customizing the model architecture or interpretability measures based on the characteristics of the application area.

The DCIts model represents a significant advancement in interpretable deep learning for multivariate time series forecasting. By combining accurate predictions with inherent interpretability, it offers a powerful tool for understanding and modeling dynamic systems. The ability to extract meaningful insights from the model’s parameters makes it particularly valuable in domains where explainability is essential. Despite certain limitations, the model’s strengths in capturing complex interactions and providing transparent explanations highlight its potential for widespread application. Future research aimed at addressing the identified limitations will further enhance the model’s utility and impact across various fields.

Authorship contribution statement

Domjan Barić: Writing – review & editing, Writing – original draft, Validation, Software, Investigation, Conceptualization. **Davor Horvatić:** Writing – review & editing, Writing – original draft, Visualization, Validation, Supervision, Methodology, Investigation, Conceptualization.

Acknowledgement

D.H. acknowledges support and funding by QuantiX—Lie Center of Excellence, and Croatian Science Foundation (HRZZ) project IP-2022-10-1648. The authors thank Dario Bojanjac and Bartol Pavlović for useful discussions.

Appendix A. Benchmarking datasets

The benchmarking datasets used in this study were sourced from Barić et al. [2]. Below, we provide detailed descriptions of all the datasets utilized in this work. The models used for benchmarking increase in complexity with each dataset, starting from a constant time series (Dataset 1) and progressing through various stages: autoregressive (Dataset 2), nonlinear autoregressive with no interactions between time series (Dataset 3), two interdependent time series (Dataset 4), linear (Dataset 5), and nonlinear autoregressive (Dataset 6) with all subsequent time series derived from the first, custom vector autoregression model (Dataset 7), and a switching time series (Dataset 8). Dataset 8 was adjusted relative to the one presented in [2], with the first time series now incorporating the switching process to test the DCIts.

Name	Model	Parameters
Dataset 1	$X_{n,t} = \alpha_n^{\text{gt}} + \epsilon_{n,t}$	$\alpha_n^{\text{gt}} = N(0, 1)$
Dataset 2	$X_{n,t} = \alpha_{n,n,l}^{\text{gt}} X_{n,t-l} + \epsilon_{n,t}$	$\alpha_{n,n,3}^{\text{gt}} = \alpha_{n,n,7}^{\text{gt}} = 1/2$
Dataset 3	$X_{n,t} = \tanh(\alpha_{n,n,l}^{\text{gt}} X_{n,t-l}) + \epsilon_{n,t}$	$\alpha_{n,n,3}^{\text{gt}} = \frac{5}{7}, \alpha_{n,n,7}^{\text{gt}} = \alpha_{n,n,9}^{\text{gt}} = \frac{1}{7}$
Dataset 4	$X_{1,t} = \alpha_{1,2,l}^{\text{gt}} X_{2,t-l} + \epsilon_{1,t}$ $X_{2,t} = \alpha_{2,1,l}^{\text{gt}} X_{1,t-l} + \epsilon_{2,t}$	$\alpha_{1,2,2}^{\text{gt}} = \alpha_{1,2,9}^{\text{gt}} = \frac{2}{5}, \alpha_{1,2,5}^{\text{gt}} = \frac{1}{5}$ $\alpha_{2,1,2}^{\text{gt}} = \alpha_{2,1,9}^{\text{gt}} = \frac{2}{5}, \alpha_{2,1,5}^{\text{gt}} = \frac{1}{5}$
Dataset 5	$X_{n,t} = \alpha_{n,1,l}^{\text{gt}} X_{1,t-l} + \epsilon_{n,t}$	$\alpha_{1,1,3}^{\text{gt}} = \frac{1}{2}, \alpha_{1,1,4}^{\text{gt}} = \frac{1}{2}$ $\alpha_{2,1,9}^{\text{gt}} = 1$ $\alpha_{3,1,2}^{\text{gt}} = \frac{1}{2}, \alpha_{3,1,7}^{\text{gt}} = \frac{1}{2}$ $\alpha_{4,1,3}^{\text{gt}} = \frac{1}{10}, \alpha_{4,1,4}^{\text{gt}} = \frac{1}{10}, \alpha_{4,1,8}^{\text{gt}} = \frac{4}{5}$ $\alpha_{5,1,2}^{\text{gt}} = \frac{1}{3}, \alpha_{5,1,5}^{\text{gt}} = \frac{2}{9}, \alpha_{5,1,8}^{\text{gt}} = \frac{4}{9}$
Dataset 6	$X_{n,t} = \tanh(\alpha_{n,1,l}^{\text{gt}} X_{1,t-l}) + \epsilon_{n,t}$	Identical to Dataset 5
Dataset 7	$X_{1,t} = \alpha_{1,1,1}^{\text{gt}} X_{1,t-1} + \alpha_{1,1,5}^{\text{gt}} X_{1,t-5} + \epsilon_{1,t}$ $X_{2,t} = 1 + \alpha_{2,1,2}^{\text{gt}} X_{1,t-2} + \epsilon_{2,t}$ $X_{3,t} = \alpha_{3,2,1}^{\text{gt}} X_{2,t-1} + \alpha_{3,4,4}^{\text{gt}} X_{4,t-4} + \epsilon_{3,t}$ $X_{4,t} = 1 + \alpha_{4,3,4}^{\text{gt}} X_{3,t-4} + \alpha_{4,5,1}^{\text{gt}} X_{5,t-1} + \epsilon_{4,t}$ $X_{5,t} = \alpha_{5,5,4}^{\text{gt}} X_{5,t-4} + \alpha_{5,2,1}^{\text{gt}} X_{2,t-1} + \epsilon_{5,t}$	$\alpha_{1,1,1}^{\text{gt}} = \frac{1}{4}, \alpha_{1,1,5}^{\text{gt}} = \frac{3}{4}$ $\alpha_{2,1,2}^{\text{gt}} = -1$ $\alpha_{3,2,1}^{\text{gt}} = 1, \alpha_{3,4,4}^{\text{gt}} = 1$ $\alpha_{4,3,4}^{\text{gt}} = -\frac{2}{7}, \alpha_{4,5,1}^{\text{gt}} = -\frac{5}{7}$ $\alpha_{5,5,4}^{\text{gt}} = \frac{12}{22}, \alpha_{5,2,1}^{\text{gt}} = \frac{10}{22}$
Dataset 8	if $X_{1,t-5} > \frac{1}{2}$: $X_{1,t} = b_{\text{high}} + \epsilon_{1,t}$ $X_{2,t} = \alpha_{2,1,5}^{\text{gt}} X_{1,t-5} + \epsilon_{2,t}$ $X_{3,t} = \alpha_{3,1,4}^{\text{gt}} X_{1,t-4} + \epsilon_{3,t}$ $X_{4,t} = \alpha_{4,4,1}^{\text{gt}} X_{4,t-1} + \alpha_{4,4,4}^{\text{gt}} X_{4,t-4} + \epsilon_{4,t}$ else: $X_{1,t} = b_{\text{low}} + \epsilon_{1,t}$ $X_{2,t} = \alpha_{2,4,2}^{\text{gt}} X_{4,t-2} + \epsilon_{2,t}$ $X_{3,t} = \alpha_{3,4,4}^{\text{gt}} X_{4,t-4} + \epsilon_{3,t}$ $X_{4,t} = \alpha_{4,4,1}^{\text{gt}} X_{4,t-1} + \alpha_{4,4,4}^{\text{gt}} X_{4,t-4} + \epsilon_{4,t}$	$\alpha_{2,1,5}^{\text{gt}} = \frac{4}{5}, \alpha_{2,4,2}^{\text{gt}} = \frac{2}{3}$ $\alpha_{3,1,4}^{\text{gt}} = \frac{2}{3}, \alpha_{3,4,4}^{\text{gt}} = \frac{4}{5}$ $\alpha_{4,4,1}^{\text{gt}} = \frac{1}{2}, \alpha_{4,4,4}^{\text{gt}} = \frac{2}{5}$ $b_{\text{high}} = \frac{7}{10}, b_{\text{low}} = \frac{2}{10}$ b_{high} and b_{low} switch, based on a persistence duration, P . $P \sim \max(P_{\text{min}}, \mathcal{N}(\mu_P, \sigma_P))$

References

- [1] S.-A. Chen, C.-L. Li, S. O. Arik, N. C. Yoder, T. Pfister, TSMixer: An all-MLP architecture for time series forecasting, *Transactions on Machine Learning Research* (2023). URL: <https://openreview.net/forum?id=wbpxTuXgm0>.
- [2] D. Barić, P. Fumić, D. Horvatić, T. Lipic, Benchmarking attention-based interpretability of deep learning in multivariate time series predictions, *Entropy* 23 (2021). URL: <https://www.mdpi.com/1099-4300/23/2/143>.
- [3] K. Fauvel, V. Masson, É. Fromont, A performance-explainability framework to benchmark machine learning methods: Application to multivariate time series classifiers, *arXiv preprint arXiv:2005.14501* (2020).
- [4] T. Guo, T. Lin, N. Antulov-Fantulin, Exploring interpretable lstm neural networks over multi-variable data, 2019. *arXiv:1905.12034*.
- [5] O. Ozyegen, I. Ilic, M. Cevik, Evaluation of interpretability methods for multivariate time series forecasting, *Applied Intelligence* 52 (2022) 4727–4743. URL: <https://doi.org/10.1007/s10489-021-02662-2>. doi:10.1007/s10489-021-02662-2.
- [6] U. Schlegel, D. V. Lam, D. A. Keim, D. Seebacher, TS-MULE: local interpretable model-agnostic explanations for time series forecast models, *CoRR abs/2109.08438* (2021). URL: <https://arxiv.org/abs/2109.08438>. *arXiv:2109.08438*.
- [7] S. M. Lundberg, S.-I. Lee, A unified approach to interpreting model predictions, in: *Advances in neural information processing systems*, 2017, pp. 4765–4774.
- [8] U. Schlegel, D. Oelke, D. A. Keim, M. El-Assady, An empirical study of explainable AI techniques on deep learning models for time series tasks, *CoRR abs/2012.04344* (2020). URL: <https://arxiv.org/abs/2012.04344>. *arXiv:2012.04344*.
- [9] T. Gangopadhyay, S. Y. Tan, Z. Jiang, R. Meng, S. Sarkar, Spatiotemporal attention for multivariate time series prediction and interpretation, *CoRR abs/2008.04882* (2020). URL: <https://arxiv.org/abs/2008.04882>. *arXiv:2008.04882*.

- [10] A.-D. Pham, A. Kuestenmacher, P. G. Ploeger, Tsem: Temporally-weighted spatiotemporal explainable neural network for multivariate time series, in: K. Arai (Ed.), *Advances in Information and Communication*, Springer Nature Switzerland, Cham, 2023, pp. 183–204.
- [11] B. Wu, L. Wang, Y.-R. Zeng, Interpretable tourism demand forecasting with temporal fusion transformers amid covid-19, *Applied Intelligence* 53 (2023) 14493–14514. URL: <https://doi.org/10.1007/s10489-022-04254-0>. doi:10.1007/s10489-022-04254-0.
- [12] L. Pantiskas, K. Verstoep, H. Bal, Interpretable multivariate time series forecasting with temporal attention convolutional neural networks, in: *2020 IEEE Symposium Series on Computational Intelligence (SSCI)*, 2020, pp. 1687–1694. doi:10.1109/SSCI47803.2020.9308570.
- [13] S. Feng, C. Miao, K. Xu, J. Wu, P. Wu, Y. Zhang, P. Zhao, Multi-scale attention flow for probabilistic time series forecasting, 2023. [arXiv:2205.07493](https://arxiv.org/abs/2205.07493).
- [14] I. Gandin, A. Scagnetto, S. Romani, G. Barbati, Interpretability of time-series deep learning models: A study in cardiovascular patients admitted to intensive care unit, *Journal of Biomedical Informatics* 121 (2021) 103876. URL: <https://www.sciencedirect.com/science/article/pii/S1532046421002057>. doi:<https://doi.org/10.1016/j.jbi.2021.103876>.
- [15] S. Jain, B. C. Wallace, Attention is not explanation, *CoRR* abs/1902.10186 (2019). URL: <http://arxiv.org/abs/1902.10186>. [arXiv:1902.10186](https://arxiv.org/abs/1902.10186).
- [16] S. Wiegrefe, Y. Pinter, Attention is not not explanation, *CoRR* abs/1908.04626 (2019). URL: <http://arxiv.org/abs/1908.04626>. [arXiv:1908.04626](https://arxiv.org/abs/1908.04626).
- [17] B. N. Oreshkin, D. Carпов, N. Chapados, Y. Bengio, N-BEATS: neural basis expansion analysis for interpretable time series forecasting, *CoRR* abs/1905.10437 (2019). URL: <http://arxiv.org/abs/1905.10437>. [arXiv:1905.10437](https://arxiv.org/abs/1905.10437).
- [18] K. Rasul, A. Sheikh, I. Schuster, U. Bergmann, R. Vollgraf, Multivariate probabilistic time series forecasting via conditioned normalizing

- flows, CoRR abs/2002.06103 (2020). URL: <https://arxiv.org/abs/2002.06103>. arXiv:2002.06103.
- [19] L. Munkhdalai, T. Munkhdalai, V.-H. Pham, M. Li, K. H. Ryu, N. Theera-Umpon, Recurrent neural network-augmented locally adaptive interpretable regression for multivariate time-series forecasting, *IEEE Access* 10 (2022) 11871–11885. doi:10.1109/ACCESS.2022.3145951.
- [20] M. Panja, T. Chakraborty, U. Kumar, A. Hadid, Probabilistic autoregressive neural networks for accurate long-range forecasting, in: B. Luo, L. Cheng, Z.-G. Wu, H. Li, C. Li (Eds.), *Neural Information Processing*, Springer Nature Singapore, Singapore, 2024, pp. 457–477.
- [21] K. Fauvel, T. Lin, V. Masson, É. Fromont, A. Termier, XCM: an explainable convolutional neural network for multivariate time series classification, CoRR abs/2009.04796 (2020). URL: <https://arxiv.org/abs/2009.04796>. arXiv:2009.04796.
- [22] R. Assaf, A. Schumann, Explainable deep neural networks for multivariate time series predictions., in: *IJCAI, 2019*, pp. 6488–6490.
- [23] J. Wang, Z. Wang, J. Li, J. Wu, Multilevel wavelet decomposition network for interpretable time series analysis, CoRR abs/1806.08946 (2018). URL: <http://arxiv.org/abs/1806.08946>. arXiv:1806.08946.
- [24] M. Castro, P. R. Mendes Júnior, A. Soriano-Vargas, R. de Oliveira Werneck, M. Moreira Gonçalves, L. Lusquino Filho, R. Moura, M. Zampieri, O. Linares, V. Ferreira, A. Ferreira, A. Davólio, D. Schiozer, A. Rocha, Time series causal relationships discovery through feature importance and ensemble models, *Scientific Reports* 13 (2023). URL: <http://dx.doi.org/10.1038/s41598-023-37929-w>. doi:10.1038/s41598-023-37929-w.
- [25] X. Dang, S. Y. Shah, P. Zerfos, seq2graph: Discovering dynamic dependencies from multivariate time series with multi-level attention, CoRR abs/1812.04448 (2018). URL: <http://arxiv.org/abs/1812.04448>. arXiv:1812.04448.

- [26] Y. Qin, D. Song, H. Chen, W. Cheng, G. Jiang, G. W. Cottrell, A dual-stage attention-based recurrent neural network for time series prediction, CoRR abs/1704.02971 (2017). URL: <http://arxiv.org/abs/1704.02971>. arXiv:1704.02971.
- [27] D. Barić, D. Horvatić, dcits, <https://github.com/hc-xai/dcits>, 2024. Maintained by the authors, Accessed: January 6th 2025.